THE ASTROPHYSICAL JOURNAL, 292:733–751, 1985 May 15

DUAL FREQUENCY OBSERVATIONS OF SOLAR MICROWAVE BURSTS USING THE VLA

R. K. SHEVGAONKAR[1] AND M. R. KUNDU
Astronomy Program, University of Maryland, College Park
Received 1984 July 30; accepted 1984 November 27

ABSTRACT

Simultaneous observations at 2 and 6 cm wavelengths of a solar active region and of microwave bursts were carried out with the Very Large Array. We find that the quiescent 6 cm emission is strongly associated with photospheric sunspots and is dominated by gyroresonance radiation. The emission at 2 cm, on the other hand, is due to free-free mechanism, and it originates from the chromosphere-corona transition region. From the degree of polarization at the two wavelengths, the magnetic field is estimated in different parts of the active region as 1000–1500 G.

The bursts observed could be divided into two categories depending on their spatial location and the relative times of maxima at the two wavelengths. The 6 cm burst emission is always spatially located close to the magnetic neutral line, whereas the corresponding 2 cm emission could be either cospatial with the 6 cm source at the top of a flaring loop or near the footpoints of the loop. We interpret the observations in terms of a two-component flare model involving both thermal and nonthermal electrons. During a flare there is bulk heating of the plasma to high temperatures as well as acceleration of the electrons. The 6 cm emission is dominated by the gyrosynchrotron radiation of the thermal electrons, while the 2 cm emission is due to the nonthermal electrons having a power-law energy distribution. The polarization data are used to estimate the magnetic field in the flaring region as 160–350 G. The best-fit value of the power-law index of the nonthermal energy distribution is ~ 4.

A DC electric-field flare model is invoked to explain the delay between the peaks of emission at the two wavelengths. We show that, depending on the physical conditions in the flaring region and the strength of the electric field, delays in either sense, i.e., higher frequency emission occurring earlier than the lower frequency emission and vice versa, can be observed. From the delay, the strength of the electric field at the energy release site is estimated to be 0.2–4 μstatvolt cm^{-1}.

Subject headings: interferometry — radiation mechanisms — Sun: flares

I. INTRODUCTION

High-resolution multifrequency solar observations at centimeter wavelengths can provide important information on the variation of temperature and magnetic field as a function of height above quasi-stationary active regions; they also provide information on the region of energy release during flares and consequently on their triggering mechanisms. The generating mechanism of active-region radio emission is wavelength-dependent. The high-frequency radiation (above ~ 10 GHz) and the low-frequency radiation (below ~ 1 GHz) are due to thermal bremsstrahlung (e.g., Shevgaonkar and Kundu 1984; Lang and Willson 1983), whereas for the intermediate frequencies the radiation is dominated by low harmonic gyroresonance absorption (Kundu *et al.* 1977; Velusamy and Kundu 1981; McConnell and Kundu 1983). The total intensity (I) and circular polarization (V) maps at different wavelengths can provide important information on the strength and structure of magnetic fields in the corona. Indeed, the V maps can be regarded as coronal magnetograms (Kundu *et al.* 1977).

In a flare the energy release region is usually located in the low corona, and therefore the microwave observations can be used to derive source parameters such as the ambient electron density, the magnetic field strength, and the number of gyrosynchrotron-emitting electrons. With a resolution of a few arc seconds as presently available with the VLA, it is possible to locate the flare energy release region within the complex magnetic structure of the flaring region. The observations conducted in the past (e.g., Alissandrakis and Kundu 1978; Marsh and Hurford 1980; Lang, Willson, and Felli 1981; Kundu, Schmahl, and Velusamy 1982; Willson 1983) indicate that the radio bursts are generally located over the magnetic neutral line, whereas their Hα counterparts are located in oppositely polarized regions, which are identified as the footpoints of the flaring loop. The changes in polarization structure and the degree of polarization during the preflare and impulsive phases have been exploited by Kundu *et al.* (1982) to infer the magnetic field topology in the flaring region. The observations by Kundu *et al.* (1982), Velusamy and Kundu (1982), and Kundu and Shevgaonkar (1985) have provided observational evidence for evolving magnetic structures which interact with the preexisting magnetic field structures and trigger the flare. The close association of hard X-ray bursts with the microwave bursts suggests a common origin of energetic electrons radiating in the two spectral domains. The energetic electrons escape from the energy-release region at the top and are guided along the magnetic field lines to the footpoints of the loop and produce hard X-ray bursts. Simultaneous multifrequency observations at microwaves and in hard X-rays are needed to properly understand the radiation mechanisms operating in different spectral domains and are therefore of much importance in modeling a flare. A two-component model with thermal and nonthermal particles has been proposed by Böhme *et al.* (1977); on the other hand, the dissipative thermal model (Brown, Melrose, and Spicer 1979; Dulk, Melrose, and White 1979) is also capable of explaining some observations,

[1] On leave of absence from Indian Institute of Astrophysics, Bangalore, India.

and the question of thermal versus nonthermal model is not fully resolved at present.

In this paper, we present simultaneous VLA observations of microwave bursts at 6 and 2 cm; we also discuss the observations of the active region in which the bursts occurred. Using the full-day synthesis, I and V maps of the active region have been produced. The radiation mechanisms at these wavelengths are discussed and the upper and lower bounds on the magnetic field of the active region are derived. The radiation mechanisms inferred from the observations are consistent with the previous interpretations (Kundu and Alissandrakis 1984; Shevgaonkar and Kundu 1984; Lang, Willson, and Gaizauskas 1983; Lang and Willson 1983). The bursts studied by us have multiple peaks. The two-dimensional I and V snapshot maps have been produced at 6 and 2 cm. From the brightness temperature and the degree of circular polarization, the magnetic field in the microwave burst sources has been estimated. The generating mechanisms responsible for 6 and 2 cm radiation are discussed; it is concluded that the 6 cm radiation in the bursts studied here originates from the bulk heated plasma, whereas the 2 cm radiation is due to the nonthermal particles generated in the energy-release process. Using a DC electric field model of flares, we attempt to interpret the delay between the peaks of emission at the two wavelengths. We show that depending on the strength of the electric field and the density in the flaring region, delays in either sense, i.e., the lower frequency occurring earlier than the higher frequency and vice versa, can be observed. For the first time, an estimate of the electric field in a flaring region is given using the microwave observations.

II. OBSERVATIONS AND RESULTS

Simultaneous microwave observations at 2 and 6 cm wavelengths of a flaring active region and bursts were carried out with the VLA in the C-configuration by dividing the 27 antennas into two subarrays. Fourteen antennas were used at 6 cm, and the remaining 13 were used at 2 cm. The two subarrays over a 12 hr period provided a UV coverage of 600 λ–130 kλ at 2 cm and 600 λ–60 kλ at 6 cm. The observations were performed with a receiver bandwidth of 12.5 MHz, and all the visibilities were recorded with a minimum integration time constant of 10 s. During the periods of burst observations, snapshot maps were produced every 10 s. Excluding the times during which the transient bursts occurred, the visibility data over the entire day were used to produce the active-region maps. The maps produced by Fourier transforming the visibilities were CLEANed, using the standard routines available at NRAO, and the CLEANed maps were convolved with a Gaussian beam of appropriate size. The synthesized beam was 5″ × 3″ for the active region at both wavelengths, while for the bursts it was 5″ × 3″ at 6 cm and 2″ × 1.″6 at 2 cm.

a) Active Region Observations

Figures 1 and 2 show the total intensity and circular polarization maps of the active region AR 2992 at 6 and 2 cm. The peak brightness temperatures are 2.8 × 10^6 K and 2.5 × 10^5 K

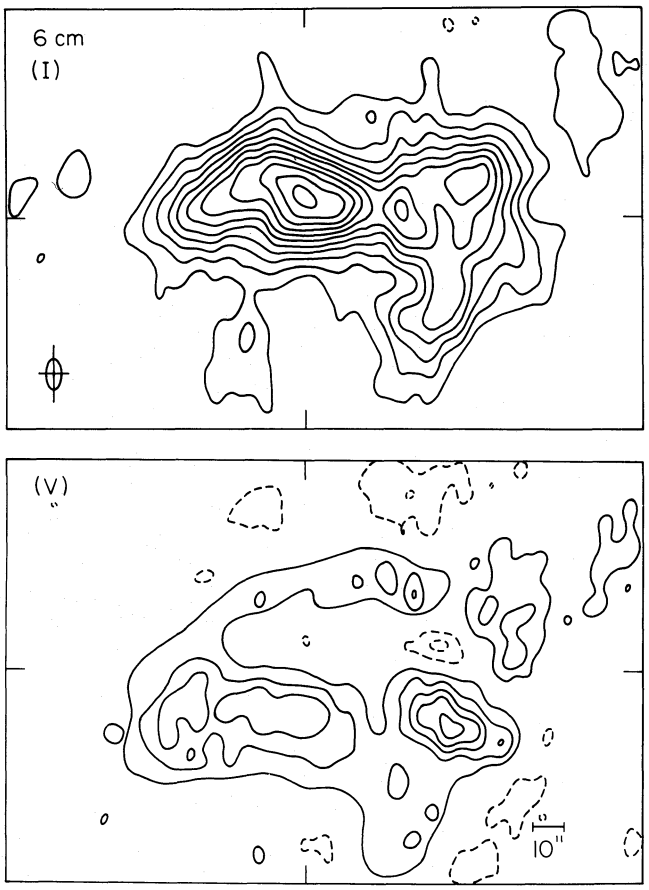

FIG. 1.—Full-day synthesis maps of the active region at 6 cm. For I map, contour interval = 2.45 × 10^5 K; for V map, contour interval = 0.91 × 10^5 K.

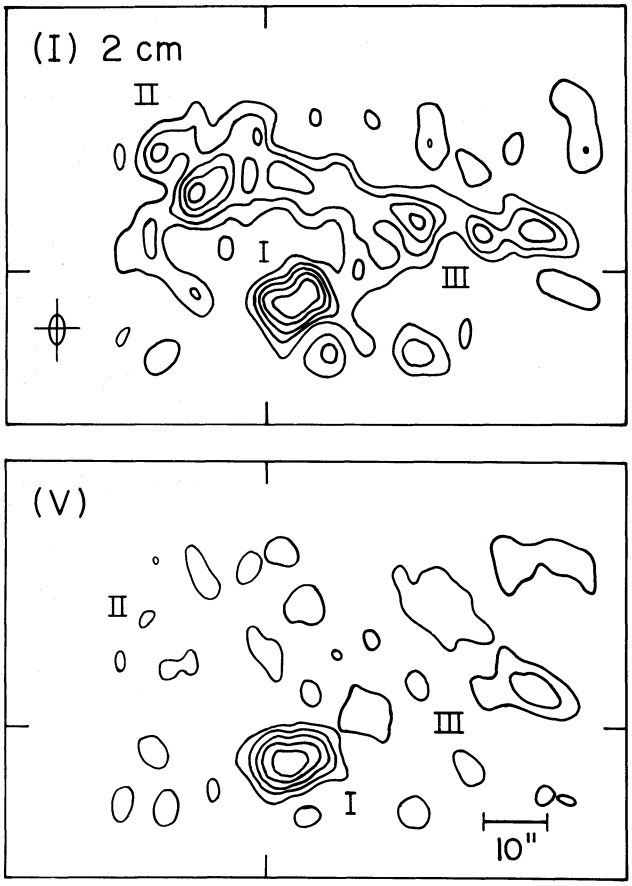

FIG. 2.—Full-day synthesis maps of the active region at 2 cm. For I map, contour interval = 4.14 × 10^4 K; for V map, contour interval = 2.07 × 10^4 K.

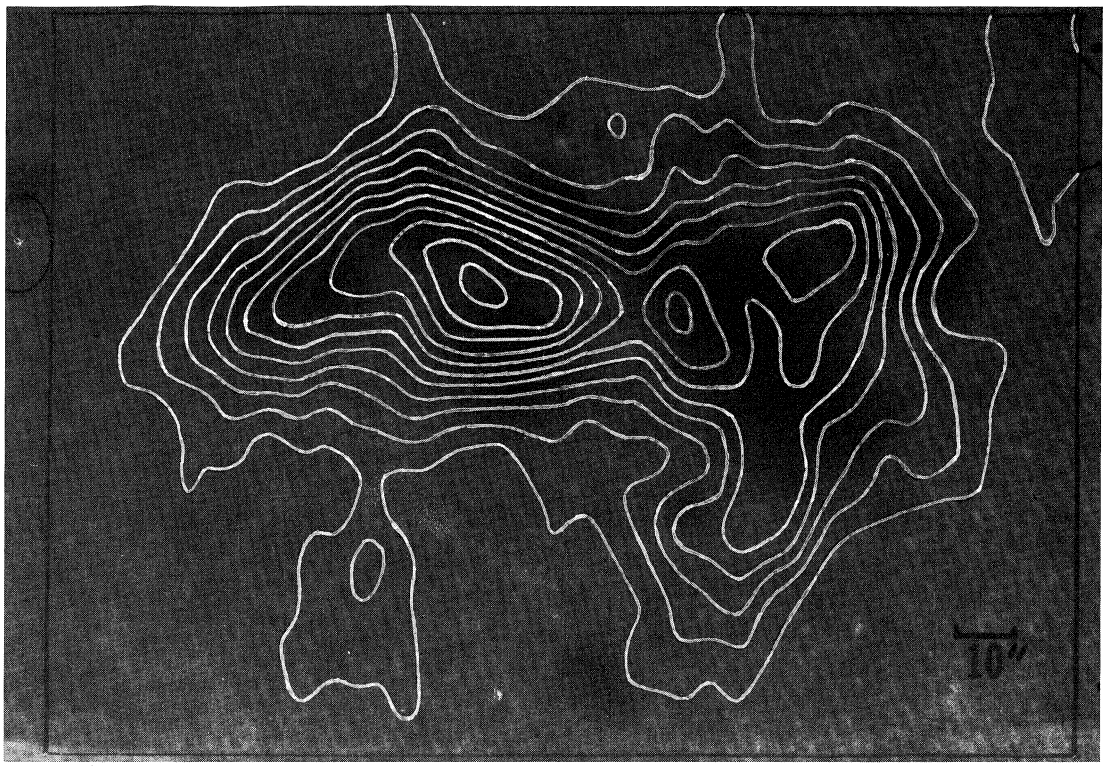

FIG. 3*a*

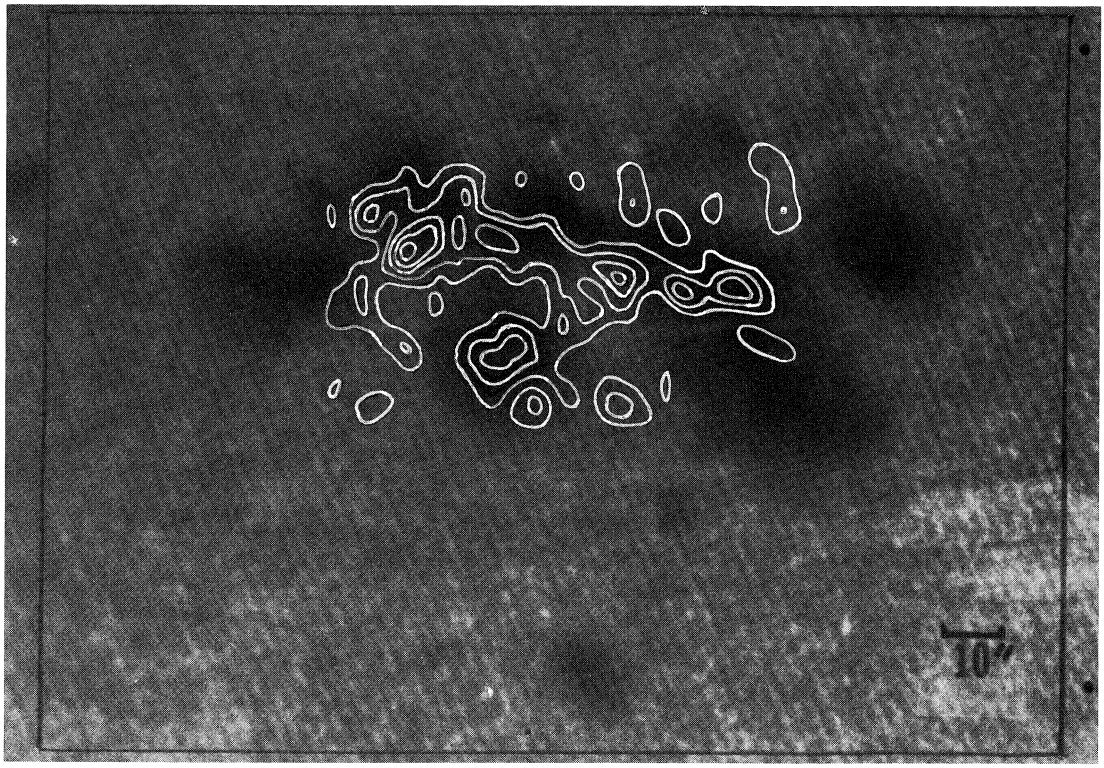

FIG. 3*b*

FIG. 3.—Superposition of the *I* map at (*a*) 6 cm and (*b*) 2 cm over off-band Hα picture

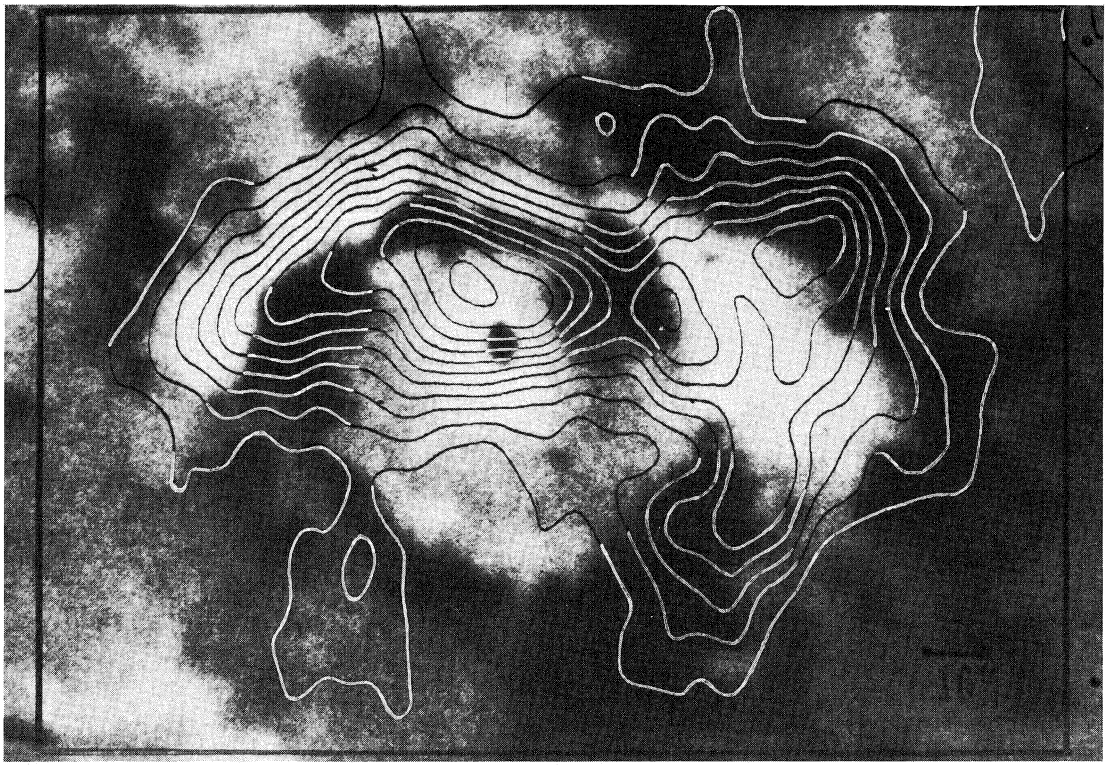

FIG. 4*a*

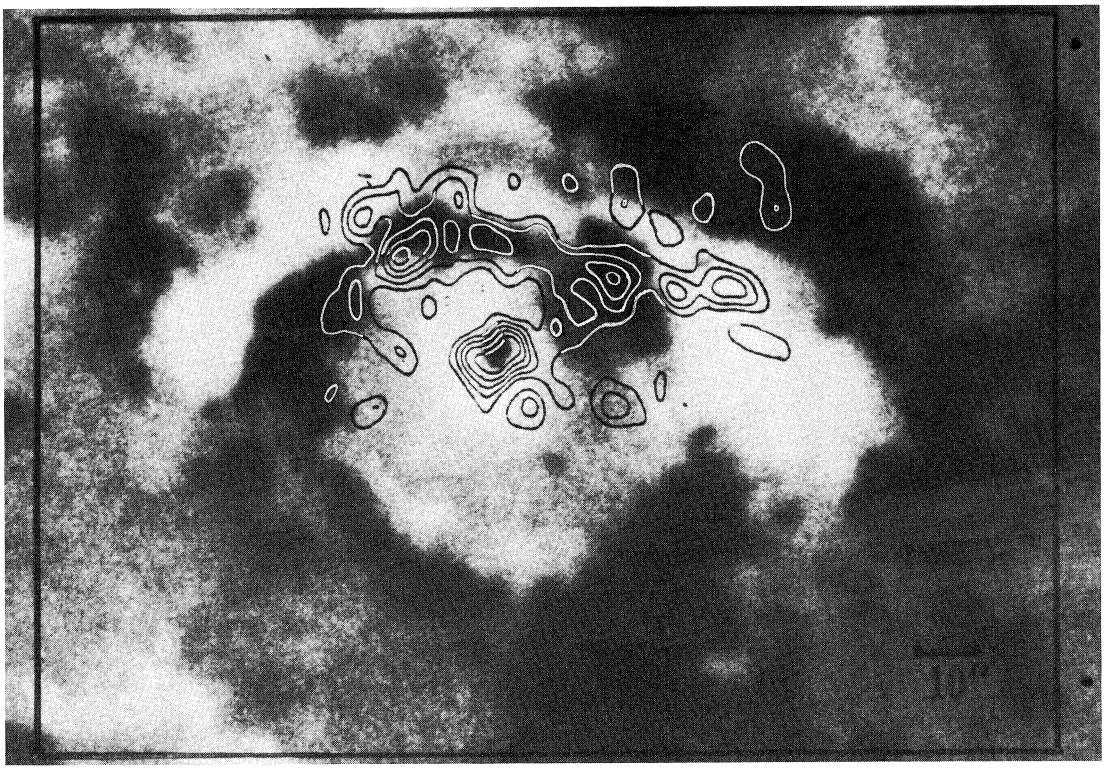

FIG. 4*b*

FIG. 4.—Superposition of the *I* map at (*a*) 6 cm and (*b*) 2 cm over KPNO magnetogram (courtesy J. Harvey)

at 6 and 2 cm respectively. The degree of circular polarization at 6 cm is ~25%, and the maximum degree of polarization occurs at the edge of the total intensity map. The polarization is negligibly small in the region where the brightness temperature is maximum. The 2 cm radiation exhibits a higher degree of circular polarization, ~50%, and the peak of the polarization spatially coincides with the total intensity maximum. Superposition of the 6 and 2 cm maps over the off-band Hα picture shown in Figure 3 indicates that the 6 cm radiation shows fairly similar structure to the underlying sunspots, whereas the agreement between the 2 cm and sunspot maps is not good, the 2 cm map being much smaller in size than the overall extent of the sunspot group. On the right side of the phase center of the map, the sources could be partly attenuated due to the small primary beam (3′) of the antenna, but on the left side the absence of sources should be real and cannot be due to attenuation by the primary-beam gain variation.

Comparison of the maps with the photospheric magnetogram (Fig. 4) reveals that the three 6 cm total-intensity peaks do not lie over the magnetic poles but more or less coincide with the magnetic neutral line. At 2 cm, the intensity peaks coincide rather well with the regions of high magnetic fields; two peaks coincide with positive polarity and the remaining peaks with the negative polarity regions. The 2 cm map essentially consists of the three regions I, II, and III. Region I originates from a strong polarity region in the magnetogram. This source has a positive circular polarization of ~50%, the polarization peak spatially coinciding with the total intensity peak. Sources II and III are complex sources, each having two strong peaks lying in oppositely polarized regions of the magnetogram. This indicates that the 2 cm radiation in sources II and III originates from the footpoints of two magnetic loops. For source II the degree of circular polarization is very small, ~12%, and for source III only one footpoint is polarized, by ~25%.

b) *Burst Observations*

On the day of observation (1981 November 13), several bursts were recorded. We present here the results of study of only two bursts, for which we had good visibility data. One burst was observed between 18:20 and 18:35 UT and a second one between 19:20 and 19:30 UT. The shortest baseline of 2000 wavelengths was used to plot the time profile of the bursts at 6 and 2 cm. Figure 5 shows the time profile of the first burst at the two wavelengths. This burst has six peaks, *A*, *B*, *C*, *D*, *E*, *F*, at 2 cm and five, *A*, *B*, *D*, *E*, *F*, at 6 cm, each lasting for about 60 s. The time profiles at 2 and 6 cm have one-to-one correspondence except that peak *C* was observed only at 2 cm without any corresponding signature at 6 cm. It is also clear from the time profiles that the first two peaks, *A* and *B*, at 6 cm occur later than the corresponding 2 cm peaks, whereas for the later three peaks, *D*, *E*, and *F*, just the reverse is true, i.e., the 6 cm radiation seems to peak before its 2 cm counterpart. Snapshot maps for every 10 s were produced over the period 18:21 to 18:35 UT. The structure of an individual burst source does not seem to change much during its rising and decaying phase; therefore only 10 s snapshot maps around the individual burst peaks are presented here. Figure 6 shows the *I* and *V* maps for all the burst peaks at 2 cm, and Figure 7 shows the corresponding *I* maps at 6 cm. At 6 cm, the observed polarization was less than ~10%; therefore the polarization maps are not presented here. The crosses in the 6 cm maps indicate the positions of the

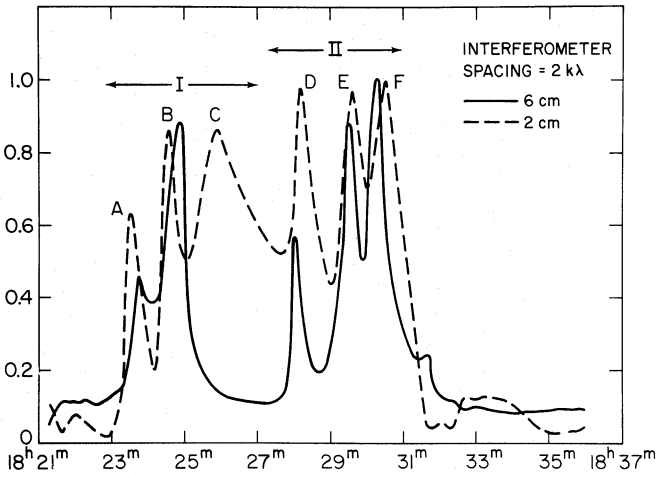

FIG. 5.—Flux vs. time profile of the first burst. At 6 cm vertical scale normalization factor is 14.0 sfu; at 2 cm scale normalization factor is 0.7 sfu.

corresponding 2 cm emission peaks. It is clear from Figure 7 that for peaks *A* and *B* the 6 and 2 cm burst sources are not cospatial. The burst peak *B* has its 6 cm *I* maximum lying between the two isolated bright components of the 2 cm burst source. Burst peak *C* at 2 cm has a structure similar to that of peak *B*; however, it rises and decays more slowly than peaks *A* and *B*, and it has no 6 cm counterpart. For the first three burst peaks *A*, *B*, and *C*, the degree of polarization is ~25% at 2 cm, and the polarization peaks spatially coincide with one of the *I* peaks. The later three burst peaks, *D*, *E*, and *F*, have somewhat different characteristics. The maxima at 6 and 2 cm are cospatial, and the 2 cm map shows a bipolar structure, with the maximum degree of polarization being ~60%. In the *V* map, the two peaks with opposite polarities lie on either side of the *I* peaks, and the polarization is essentially zero at the intensity peaks. For burst peaks *D*, *E*, and *F* there also exists a weak source in the eastern direction of the main burst source at 2 cm. There is no detectable emission from this source at 6 cm. From Figure 8 it can be seen that the 6 cm sources are always located approximately over the magnetic neutral line; however, for the 2 cm sources this is not always the case. For burst peaks *A*, *B*, and *C* the *I* peaks are spatially coincident with the high magnetic field regions of the magnetogram; and the sense of polarization is same as the underlying photospheric magnetic field. On the other hand, for burst peaks *D*, *E*, and *F*, the sources appear to be aligned more or less along the magnetic neutral line. The burst sources are bipolar; however, the two oppositely polarized regions appear to be aligned approximately parallel to the preexisting neutral line of the active region. The first three burst peaks, *A*, *B*, and *C*, and the later three burst peaks, *D*, *E*, and *F*, appear to constitute two distinct groups, for which the delays between 6 and 2 cm peaks have opposite sign; also, the structures of these two sets of burst peaks are different. Although peak *C* does not have any counterpart at 6 cm, we group it along with the first two burst peaks because it has characteristics similar to those of peak *B* at 2 cm.

The second burst consists of two peaks. The first peak is much stronger than the second one. The same burst was observed by the *SMM*-HXRBS experiment. The hard X-ray burst has a sharp rise and a comparatively slow decay. Figure 9 shows the time profiles of the burst at 6 cm, 2 cm, and in hard

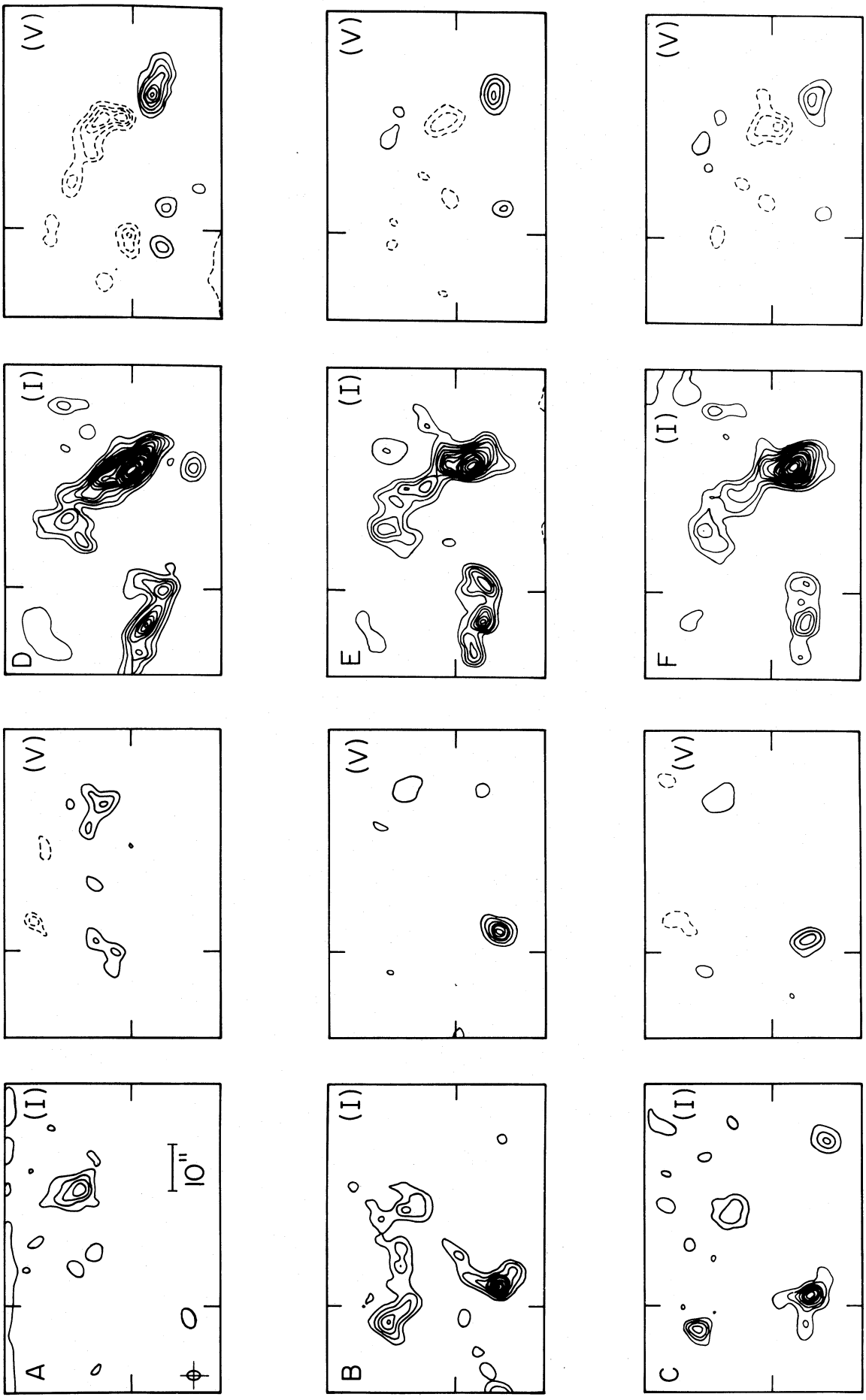

FIG. 6.—*I* and *V* maps at the peaks of the first burst at 2 cm. For *I* maps, contour interval = 9.70×10^4 K and the lowest contour is 1.94×10^5 K. For *V* maps, contour interval = 6.05×10^4 K. Maximum temperatures for the six peaks are 0.7×10^6, 1.0×10^6, 0.8×10^6, 2.1×10^6, 1.6×10^6, and 1.7×10^6 K respectively.

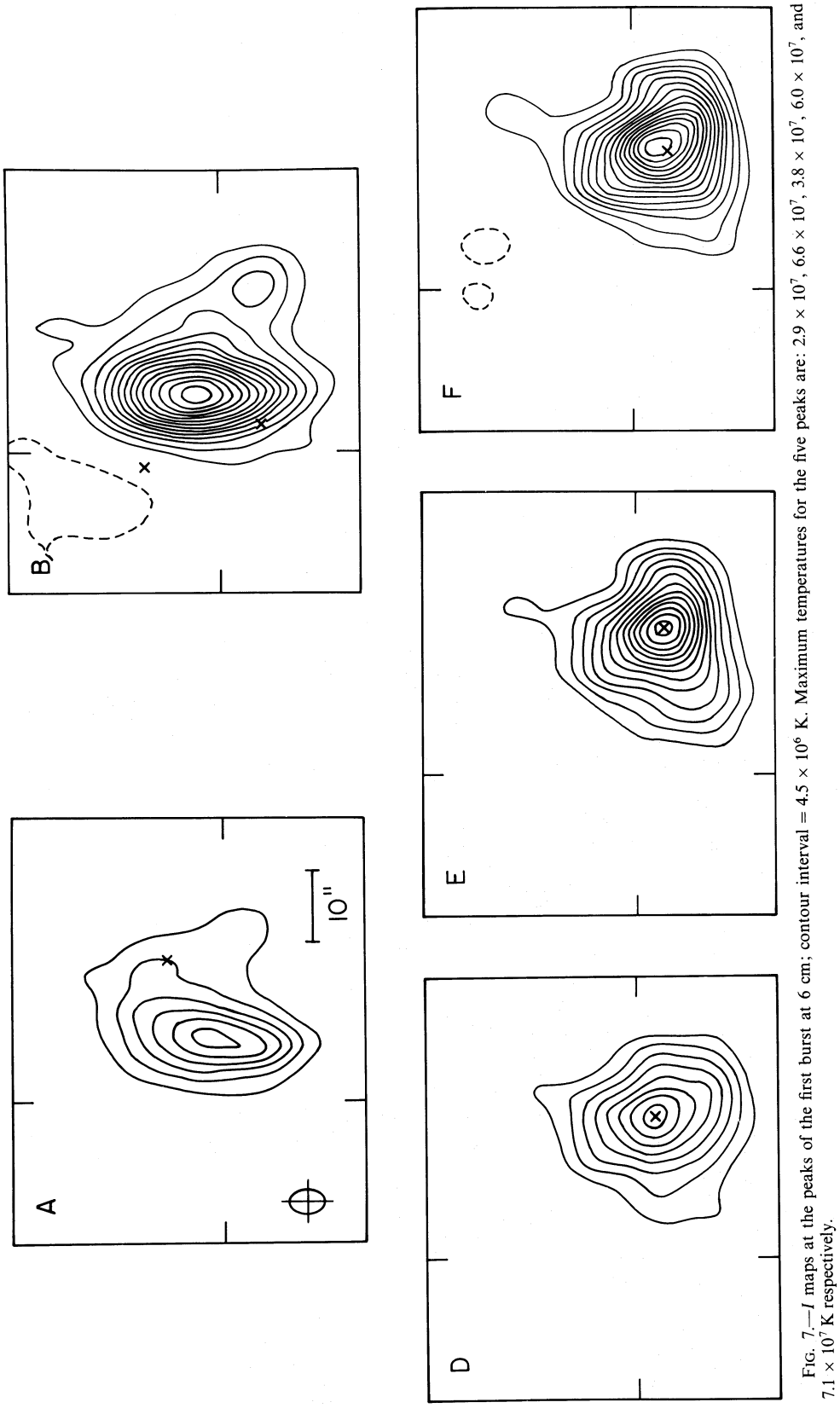

FIG. 7.—*I* maps at the peaks of the first burst at 6 cm; contour interval = 4.5×10^6 K. Maximum temperatures for the five peaks are: 2.9×10^7, 6.6×10^7, 3.8×10^7, 6.0×10^7, and 7.1×10^7 K respectively.

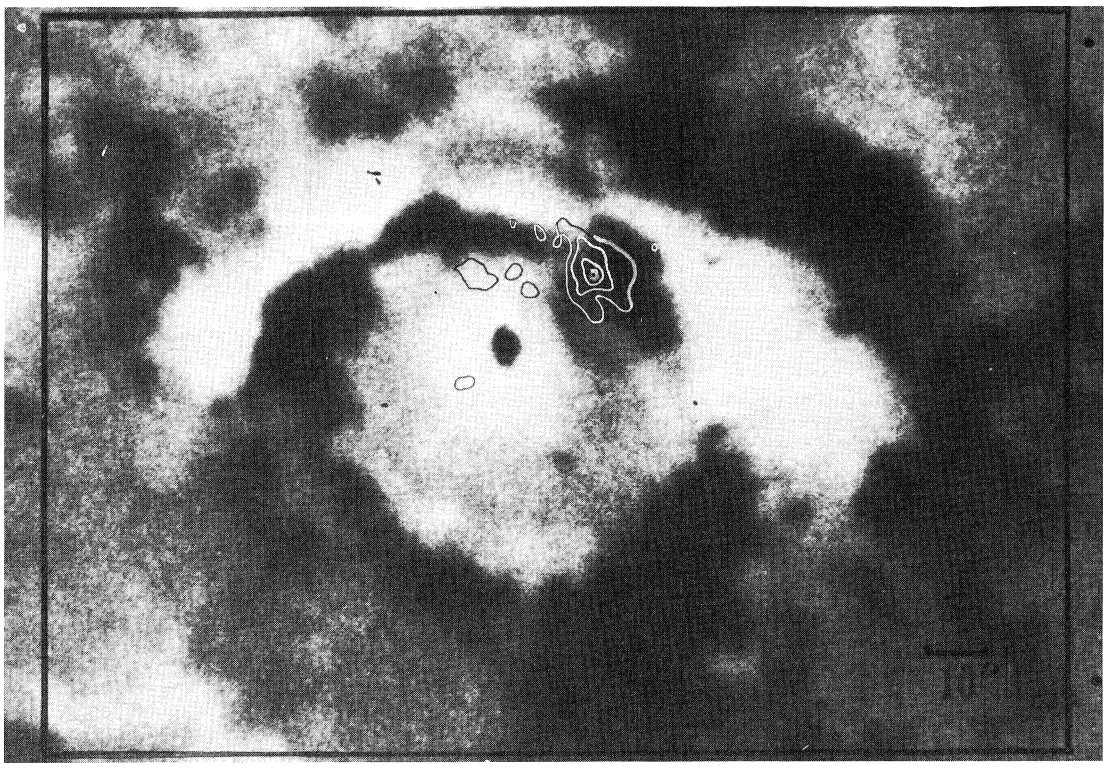

FIG. 8*a*

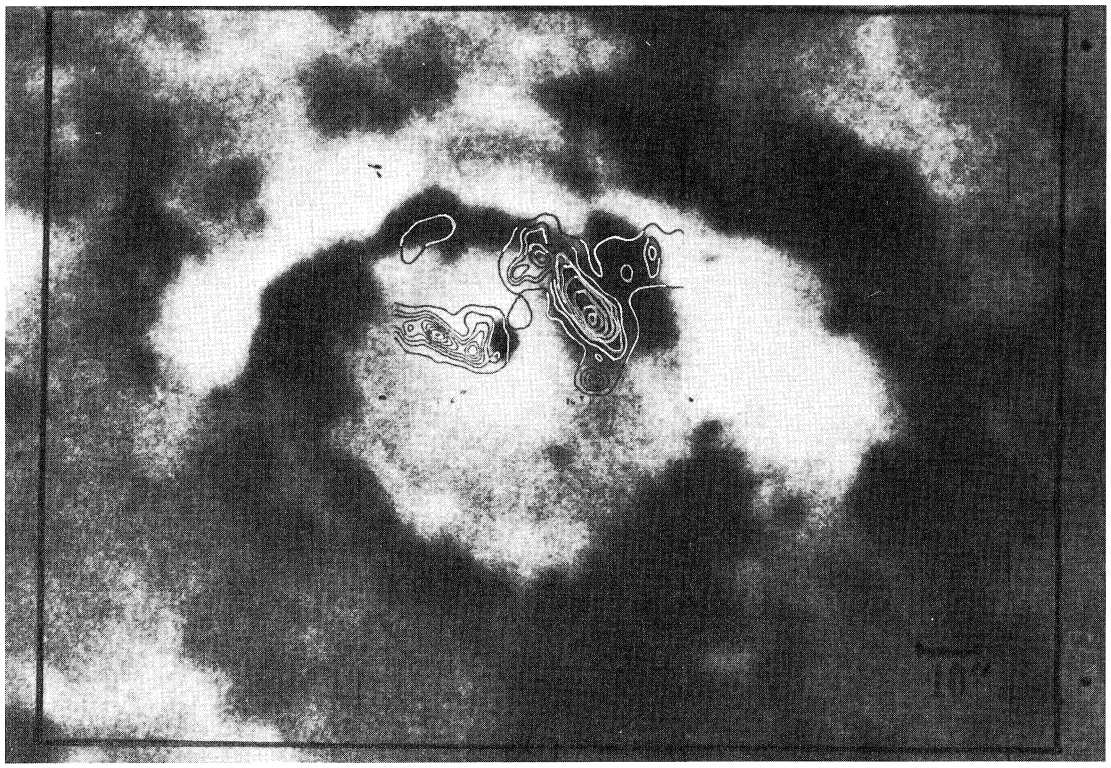

FIG. 8*d*

FIG. 8.—Superposition of *I* maps at the peaks of the first burst at 2 cm over KPNO magnetogram

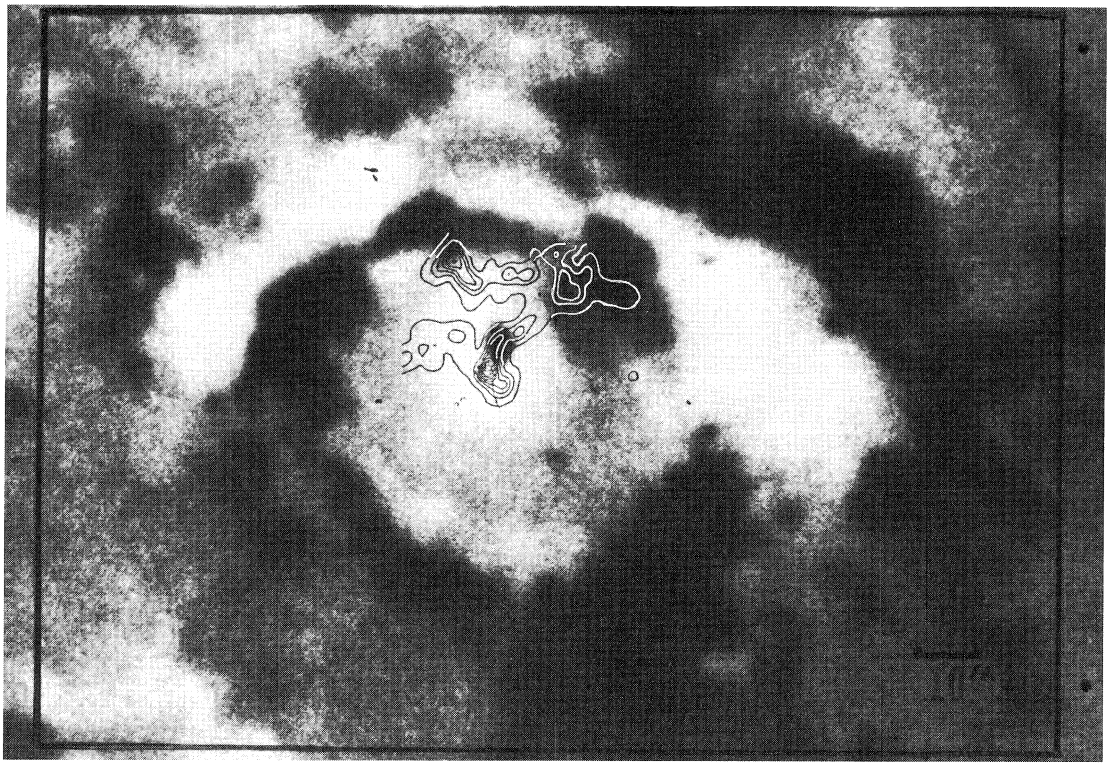

FIG. 8*b*

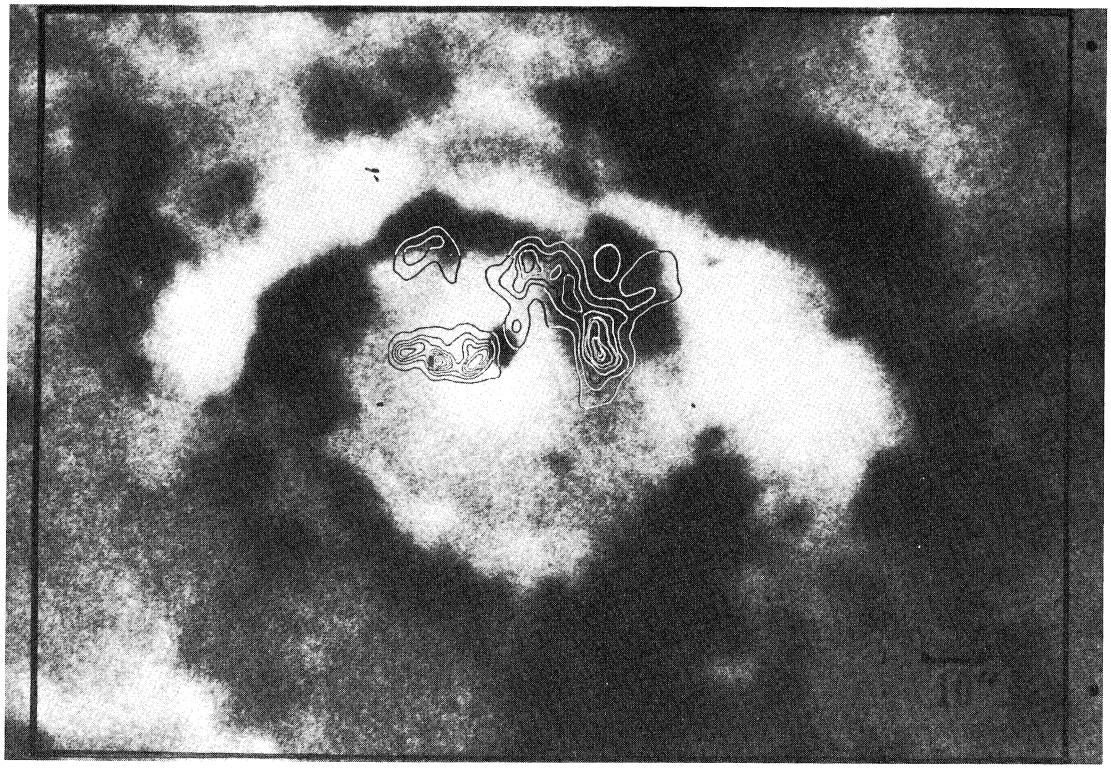

FIG. 8*e*

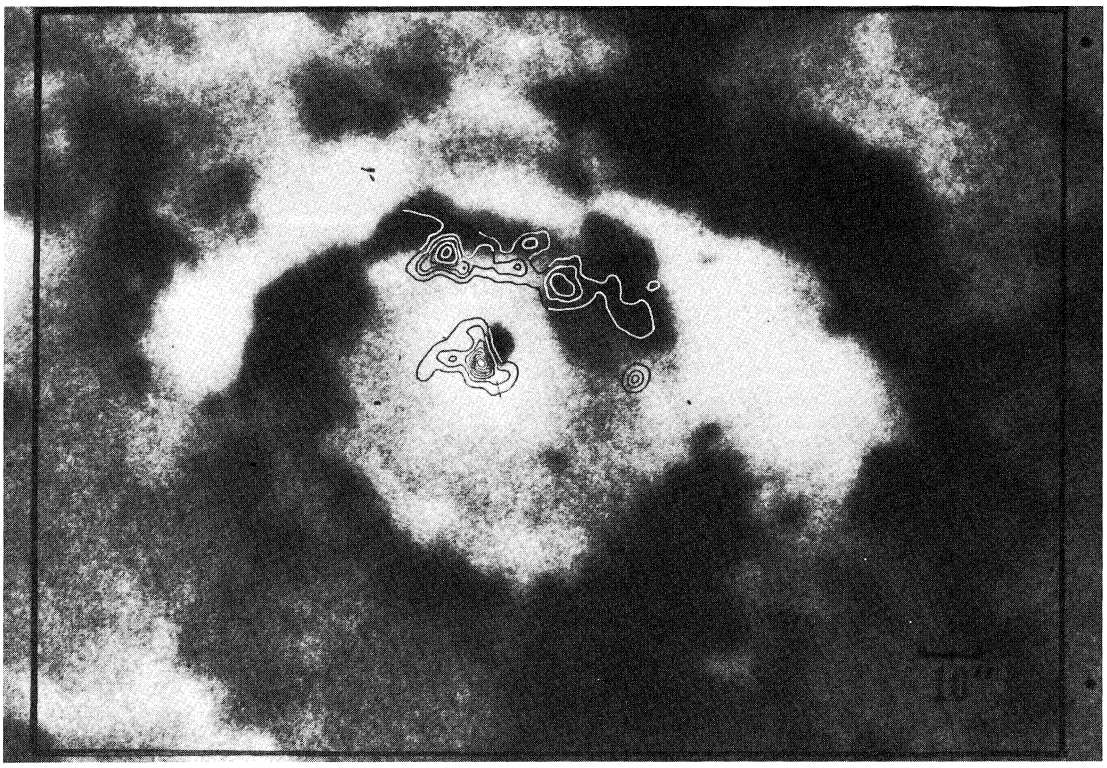

FIG. 8*c*

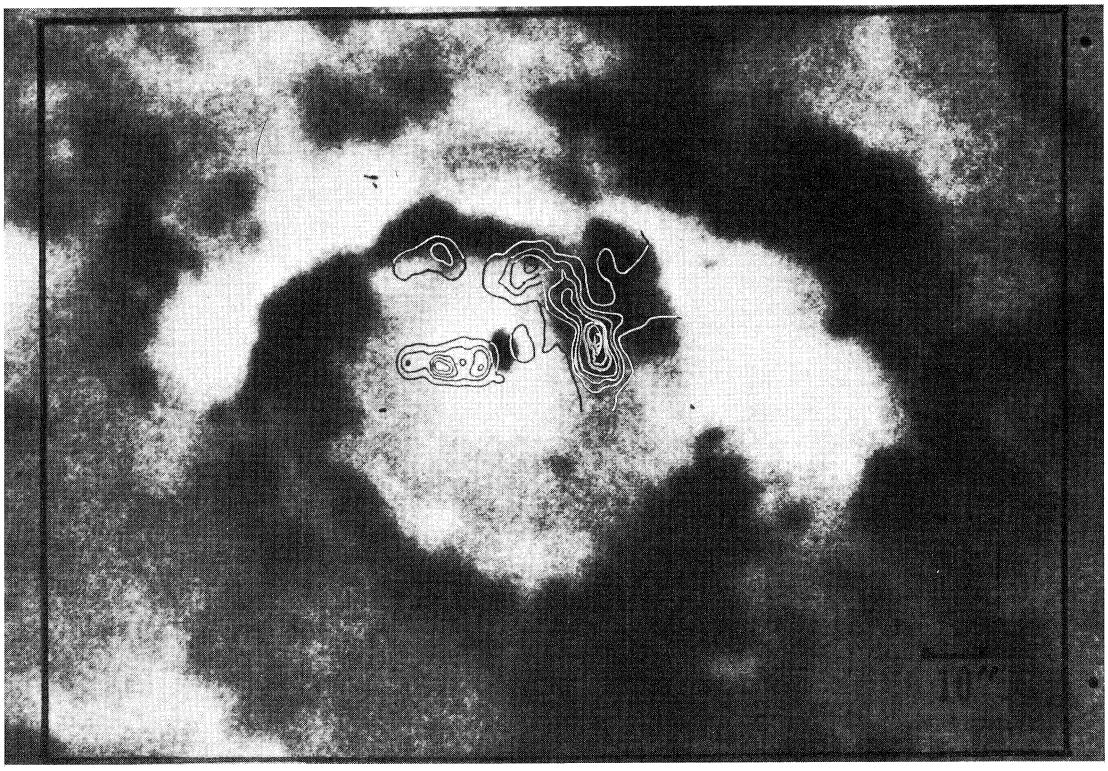

FIG. 8*f*

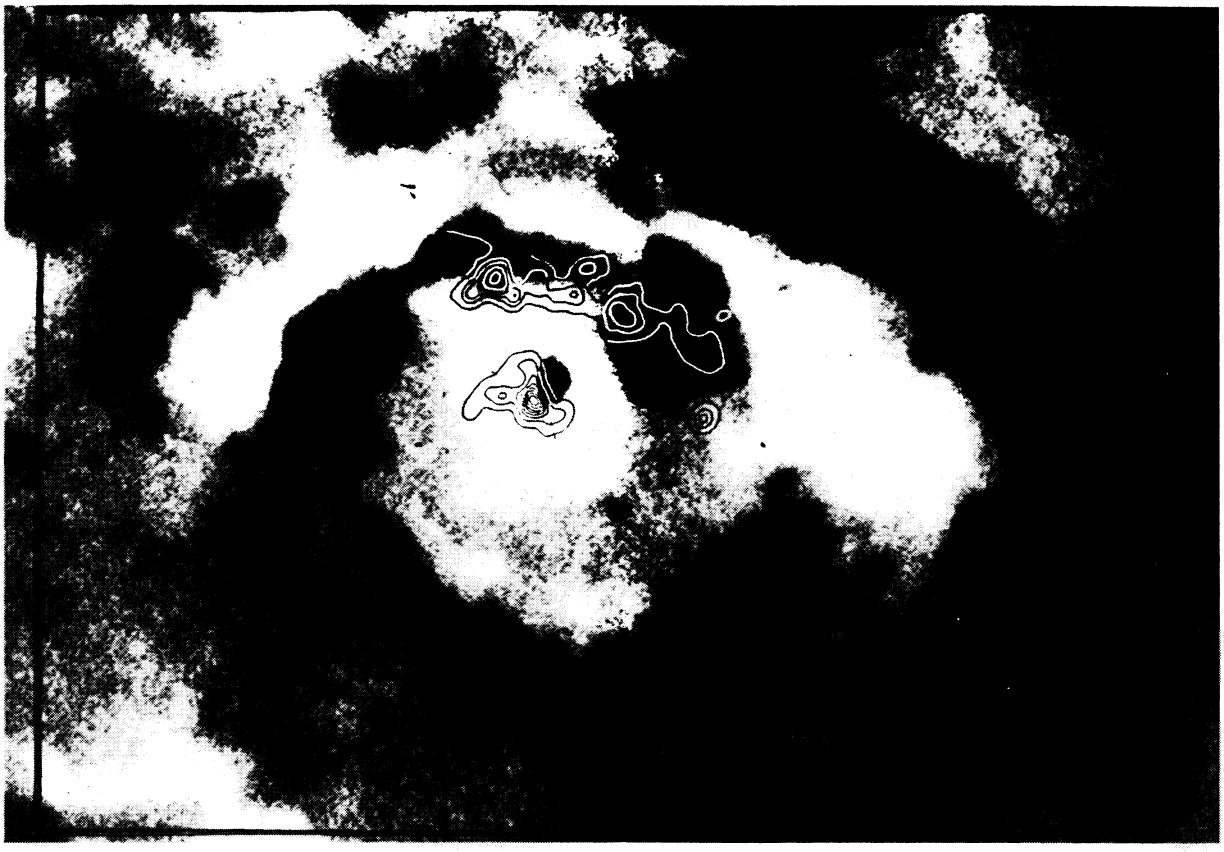

FIG. 8c

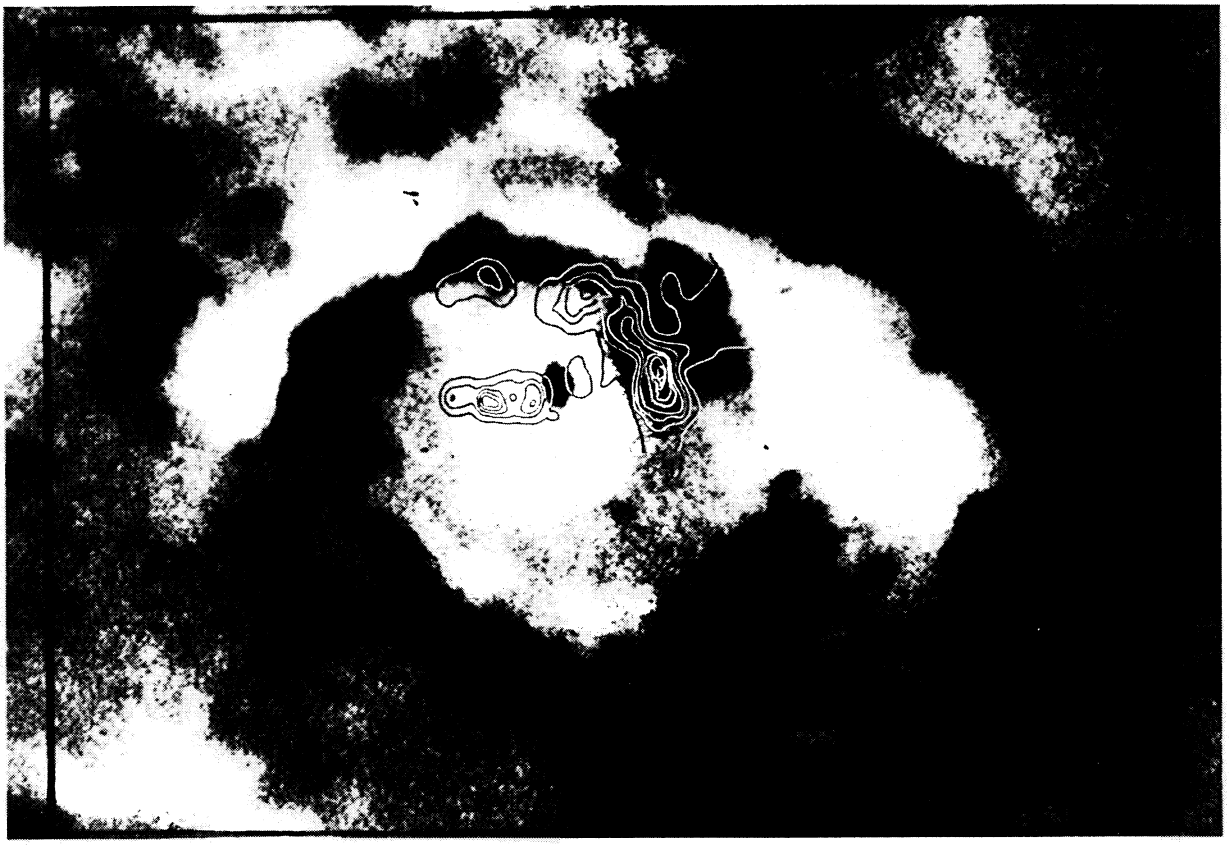

FIG. 8f

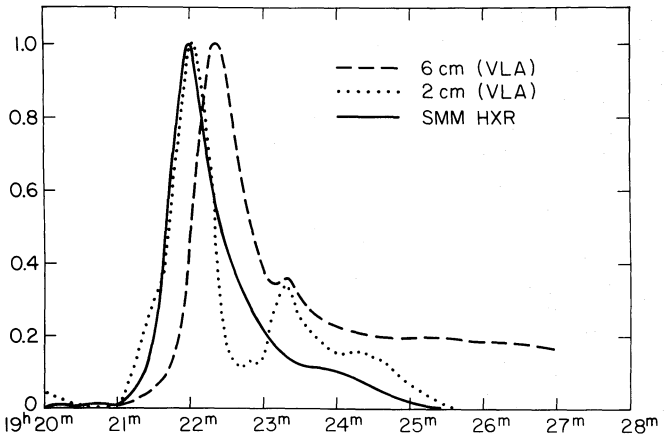

FIG. 9.—Flux vs. time profile of the second burst. At 6 and 2 cm the shortest baseline of $\sim 2k\lambda$ is used. The hard X-ray time profile in the energy range 30–60 keV is also shown. For 6 cm, the normalization factor is ~8.5 sfu and at 2 cm the normalization factor is ~0.9 sfu. For hard X-rays the maximum count is 120.

X-rays. The hard X-ray and 2 cm radiations peak more or less simultaneously, but the 6 cm intensity peaks later by ~15 s. The 2 cm and hard X-ray emissions decay to preburst levels within 3–4 min after the peak, but at 6 cm the postburst radiation exists for a much longer duration at a level of ~20% of its peak value. Figure 10 shows the 6 and 2 cm maps around the peak of the burst. It is clear from the figure that this burst

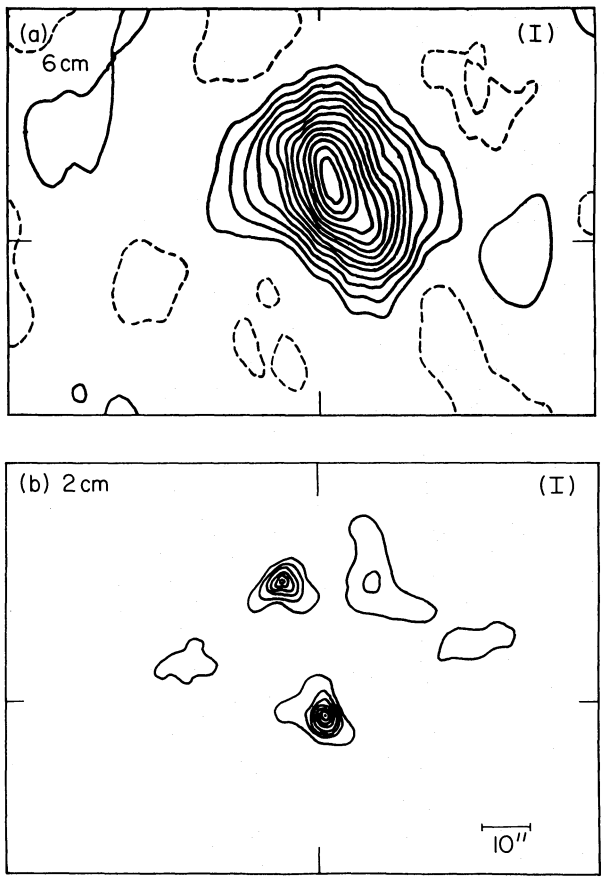

FIG. 10.—*I* maps around the stronger peak of the second burst at 6 and 2 cm. Contour interval = 2.6×10^6 K at 6 cm, 9.70×10^4 K at 2 cm.

also has characteristics similar to the first three peaks of the first burst. That is, the 6 cm emission peaks after its 2 cm counterpart; the 6 cm and 2 cm burst sources are not cospatial; the 2 cm maxima are spatially coincident with strong magnetic regions of the magnetogram; and the 6 cm burst source has its maximum located close to the magnetic neutral line, and between the two peaks of the 2 cm source. This burst will be discussed along with the first set of burst peaks of the first burst (18:20–18:35 UT).

III. DISCUSSION

a) Active Region

From the overlay of the 2 cm map over the magnetogram, it is clear that the 2 cm radiation occurs in regions of strong magnetic fields. Source I coincides with the base of a strong unipolar region in the magnetogram, and the emission from sources II and III originates from the footpoints of two magnetic loops. The brightness temperature T_B of source I is $\sim 2.5 \times 10^5$ K, and for sources II and III it is ~ 1.2–1.5×10^5 K. Computations (see Shevgaonkar and Kundu 1984) show that for such low brightness temperatures, gyroresonance absorption cannot provide the required opacity. For a magnetic scale height of $\sim 10^9$ cm, an electron temperature T_e the same as the observed T_B, an electron density $N_e \approx 10^{10}$ cm^{-3}, and the angle between the magnetic field lines and the line of sight $\theta \approx 30°$, i.e., the same as the heliocentric angle of the active region, the gyroresonance absorption even for the third harmonic is optically thin, with $\tau_x \approx 0.1$ and $\tau_0 \approx 10^{-4}$. On the other hand, assuming a source size of $\sim 5 \times 10^8$ cm and the same values of N_e and θ, the radiation due to thermal bremsstrahlung could be optically thick. Similar conclusions were reached by Shevgaonkar and Kundu (1984) and Lang, Willson, and Gaizauskas (1983). For the source parameters assumed above, an electron temperature $T_e \approx 2.5 \times 10^5$ K and a magnetic field of ~2000 G, τ_x is only ~0.5, and the observed T_B will be only $\sim 10^5$ K. By simply increasing T_e, the observed brightness temperature of 2.5×10^5 K cannot be explained, since in the optically thin domain T_B varies as $T_e^{-1/2}$. The only possible alternative is the enhancement of the electron density. An electron density of 1.5–2×10^{10} cm^{-3} is needed to make the region optically thick. If the region is optically thick in the extraordinary mode (i.e., $\tau \approx 1$), the observed polarization requires $\tau_0 \approx 0.4$, which implies a lower limit of ~1500 G for the magnetic field in the radiating source. This value of magnetic field is consistent with the photospheric magnetic field of 2200 G in that region. For sources II and III, T_B of ~ 1.2–1.5×10^5 K could be originating from regions where $N_e \approx 10^{10}$ cm^{-3} and T_e is the same as the observed T_B. The absence of polarization in source II puts a lower limit of 10^{10} cm^{-3} for N_e and an upper limit of ~1000 G for the magnetic field strength. In source III the observed polarization of ~25% over one pole requires a magnetic field of ~1500 G which is also consistent with the magnetic fields at the photospheric level in that region.

At the altitude from where the 6 cm radiation originates, taking $N_e \approx 10^9$ cm^{-3}, it can be seen that for an electron temperature $T_e > 2 \times 10^6$ K, thermal bremsstrahlung is optically thin and the radiation must be due to gyroresonance absorption. The same conclusion was derived from the previous observations of Kundu *et al.* (1977), Shevgaonkar and Kundu (1984), and Lang and Willson (1983). The 6 cm *V* map shows significant polarization only on the rim of the *I* map, probably because away from the center of the active region the optical

depth in general decreases, making both extraordinary and ordinary modes or at least the ordinary mode optically thin.

b) *Microwave Bursts*

High spatial resolution observations of microwave bursts at 6 and 2 cm can provide information on the magnetic-field topology of the region where the flare energy is released. The two sets of the burst peaks, i.e., *A*, *B*, *C* and *D*, *E*, *F*, as discussed earlier, have different source morphology. Therefore they will be discussed separately.

i) *Burst Peaks I*

Comparison of the radio maps with the photospheric magnetogram clearly indicates that the 6 cm burst source lies over the magnetic neutral line, whereas with the positional accuracy presently available it is difficult to say if the corresponding 2 cm sources are located in regions of opposite magnetic polarity. Assuming that they are, it is easy to associate the event with a single magnetic loop. However, if the northern source at 2 cm lies in the region of same polarity as the southern source, the event could be associated with multiple loops, the northern source being a miniloop by itself. In that case there must be a large loop presented between the two regions of opposite polarities, as suggested by the 6 cm burst position. Thus, if the energy is released in a large flaring loop, the 6 cm emission seems to originate from the top of the loop, while the 2 cm emission arises from the footpoints. For burst peaks *B* and *C*, one of the 2 cm sources coincides with a region of strong magnetic field in the magnetogram, and the other lies in a comparatively weaker field. This is probably similar to the case where the energy release takes place in an asymmetric loop, as discussed by Kundu and Vlahos (1979). The polarization map is also consistent with this model, which accounts for the unipolar burst radiation arising from the strong magnetic field. At 6 cm the brightness temperature T_B is ~ 3–7×10^7 K, and the degree of circular polarization is very low. This low degree of circular polarization may imply that the 6 cm emission is thermal. Before discussing this point any further, it is important to consider quantitatively the relative contributions of the thermal and nonthermal emissions in the total burst radiation.

First we shall compute the brightness due to the nonthermal particles produced in the flare. It is believed that the flare energy release region is located somewhere in the low corona, where the magnetic field is a few hundred gauss. For frequencies greater than ~ 5 GHz and magnetic fields of a few hundred gauss, the approximate formulae given by Dulk and Marsh (1982) can be used to compute the brightness temperature. For the nonthermal electrons having an isotropic pitch angle distribution, the effective electron temperature $T_{\rm eff}$, the absorption coefficient $k_{\nu \rm NT}$, and the degree of circular polarization p for the optically thin case are given by

$$k_{\nu \rm NT} \approx 1.4 \times 10^{-7.6-2.18\delta} 2.8^{1.3+0.98\delta} \times (\sin\theta)^{-0.09+0.72\delta} B_2^{0.3+0.98\delta} \nu_{10}^{-1.3-0.98\delta} N_6 , \quad (1)$$

$$T_{\rm eff} \approx 2.2 \times 10^{10-0.14\delta} 2.8^{-0.5-0.08\delta} (\sin\theta)^{-0.36-0.06\delta} \times \left(\frac{\nu_{10}}{B_2}\right)^{0.5+0.085\delta} , \quad (2)$$

$$p \approx 0.2 \times 2.8^{0.21+0.37\sin\theta} 10^{-0.42+0.05\delta-0.74\sin\theta+1.93\cos\theta-1.16\cos^2\theta} \times \left(\frac{\nu_{10}}{B_2}\right)^{-0.21-0.37\sin\theta} . \quad (3)$$

The electrons are assumed to have a power-law distribution of type $n(E) = KE^{-\delta}$, and K is related to N, the number of nonthermal electrons per cm^3 with $E > E_0$ (10 keV), by the relation $K = (\delta - 1)E_0^{\delta-1}N$, while $\nu_{10} = \nu(\rm Hz)/10^{10}$, $B_2 = B(\rm G)/10^2$, $N_6 = N(\rm cm^{-3})/10^6$, and θ is the angle between the magnetic field and the line of sight. Using formulae (1) and (2), the brightness temperature $T_B = T_{\rm eff}[1 - \exp(-k_{\nu \rm NT} L)]$ (L is the source dimension in cm) at 6 cm has been plotted against the magnetic field strength in Figure 11. The values chosen for the source parameters are $N \approx 10^6$ cm^{-3}, $\delta = 3$–5, $\theta = 25°$ and 70°, and $B = 100$–600 G. It can be seen from the plot (Fig. 11) that for reasonable parameters, the emission at 6 cm is optically thin even for magnetic fields as high as 600 G, and therefore using equation (3) one obtains a degree of circular polarization $p \gtrsim 30\%$ for a magnetic field greater than ~ 100 G. This means that the nonthermal particles if, there are any at all, are trapped near the top of the loop—cannot account for the observations which show very small polarization in the 6 cm source. The other possibility for the 6 cm radiation is that the region is heated to a high temperature of ~ 1–7×10^7 K, and the particles with a Maxwellian energy distribution produce the emission due to the gyrosynchrotron mechanism. The expression for the absorption coefficient for the mildly relativistic case is (Zheleznyakov 1970; Dulk, Melrose and White 1979):

$$k_{\nu \rm TH} = \pi^{1/2}\left(\frac{s}{2}\right)^{s+1/2} \frac{1.796 \times 10^{19} N_e}{\omega c} \times (4.811 \times 10^{-10})^s T_e^{s-1} (\sin\theta)^{2s-2} (1 \pm \cos\theta)^2 , \quad (4)$$

where $\omega = 2\pi\nu$, T_e = thermal temperature of the plasma, N_e = electron density of the thermal particles (cm^{-3}), and

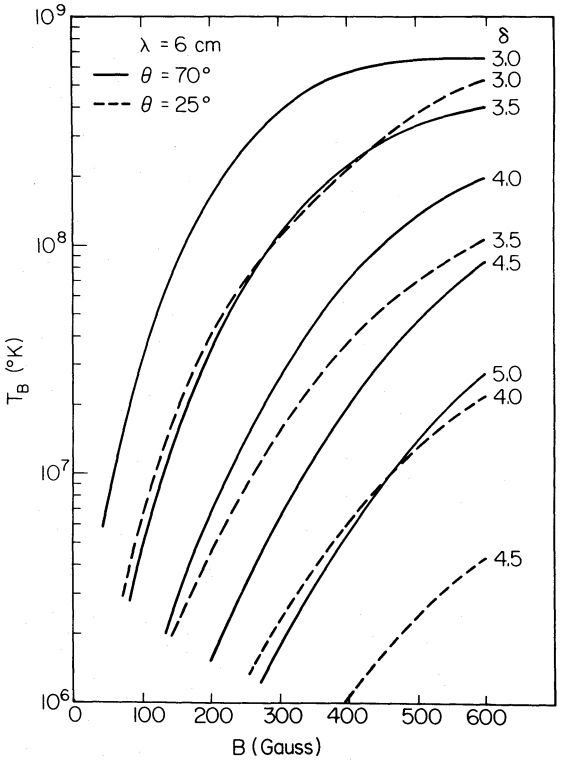

FIG. 11.—Brightness temperature due to gyrosynchrotron radiation of nonthermal electrons having a power-law energy distribution vs. magnetic field. θ is the angle between the magnetic field and the line of sight. δ = power law index of the electron energy distribution. λ = wavelength used for computation (6 cm).

s = harmonic number = $\nu/(2.8 \times 10^6 B)$. For $N_e \approx 10^{10}$ cm^{-3}, $\nu = 5$ GHz ($\lambda = 6$ cm), $\theta = 70°$ and 25°, $B = 100$–600 G, and $T_e = 1$–7×10^7 K, the brightness temperature $T_B (= T_e[1 - \exp(-k_{\nu_{TH}} L)])$ as a function of the magnetic field is plotted in Figure 12. For the temperature range 3–7×10^7 K, the radiation is optically thick for a magnetic field as low as ~ 160 G, and the degree of polarization should be zero with $T_B \approx T_e$. These computations clearly indicate that the observations presented here require that the 6 cm radiation must be caused by the bulk heating of the plasma up to temperatures of ~ 3–7×10^7 K in the energy-release region where the magnetic field is $\gtrsim 160$ G. Similar estimates of the magnetic field in the flaring region were obtained by Velusamy and Kundu (1981) from the lifetime of the electrons in the postflare loops. It should be noted that for $T_e \approx 3$–7×10^7 K, and an electron density of 10^{10} cm^{-3}, the free-free emission is negligible.

Using formulae (1), (2), and (4), one can show that at 2 cm neither thermal not nonthermal particles in the 6 cm source can produce high enough opacity due to gyrosynchrotron radiation if the magnetic field is $\lesssim 200$ G and $\delta \gtrsim 4$. Thus from the lack of spatial correspondence between the 2 cm and 6 cm burst source and the absence of circular polarization at 6 cm, we estimate a magnetic field of 160–200 G in the flaring region.

Since the 6 cm emission originates from near the top of the loop, while the 2 cm emission comes from its footpoints, the nonthermal particles with initial low pitch angle generated during the flare are probably beamed along the field lines to the footpoints of the loop. The possibility of a conduction front moving down the loop is ruled out, because in that case the 2 cm emission will peak *after* the 6 cm emission and therefore will not be consistent with the observations. The emission at 2 cm could be due either to gyrosynchrotron radiation of the beaming electrons in the high magnetic field or to low harmonic gyroresonance radiation in the thermal plasma produced by thermalization of the nonthermal electrons. However, the observed brightness temperature and polarization cannot be explained by the gyrosynchrotron mechanism. For a high magnetic field of ~ 1000 G near the footpoints of the loop, the degree of circular polarization is almost 100%, whereas the observed degree of polarization is only $\sim 40\%$. On the other hand, the alternative possibility that the emission at 2 cm is due to gyroresonance mechanism in the thermal plasma produced by thermalization of the beam of the nonthermal particles can explain the results better. Therefore, it appears that in this case, although the emission at 2 cm is not due to the gyrosynchrotron radiation of the nonthermal tail, it indirectly supports the presence of the nonthermal electrons.

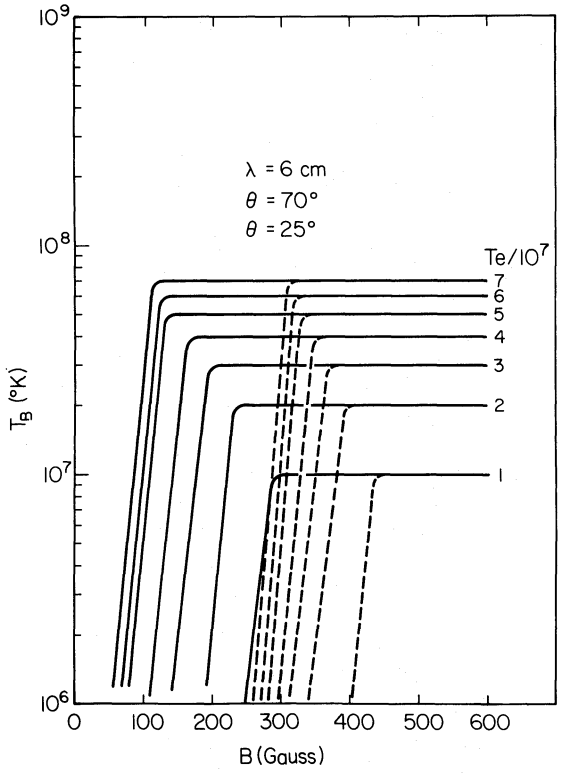

FIG. 12.—Brightness temperature due to gyrosynchrotron radiation of thermal particles with Maxwellian energy distribution vs. magnetic field. θ is the angle between the magnetic field and the line of sight. T_e is the thermal temperature of the particles. λ = wavelength used for computation (6 cm).

It may be possible now to explain why in Figure 5 there is no 6 cm burst peak corresponding to peak *C* at 2 cm. Similarity of the 2 cm maps for burst peaks *B* and *C* leads us to believe that the energy-release site is probably the same for both burst peaks, and only their temporal evolutions are different. By the same energy-release site we mean that if the 6 cm source was present for this burst peak it would have been approximately at the same position as that of the 6 cm source for peak *B*, and the absence of the 6 cm emission in this case is not due to a change in the ambient physical conditions like electron density, magnetic field, etc. It is possible that due to the long heating time, the dissipative losses last long enough to prevent the plasma from bulk heating to as high a temperature, and the temperature does not rise to more than $\sim 10^7$ K. For this electron temperature and a magnetic field of ~ 160–200 G, the radiation at 6 cm is optically thin (Fig. 12), with T_B a few times 10^6 K, which corresponds to a flux of ~ 1 sfu, less than the detection limit.

ii) *Burst Peaks II*

For burst peaks *D*, *E*, and *F* (Fig. 5), the 2 cm sources are cospatial. (The weaker eastward component is discussed later.) Like the peaks in the first set, the 6 cm sources for the second set of peaks are also located over the magnetic neutral line, and they are practically unpolarized. The 2 cm maps clearly exhibit structural changes from one burst peak to another. The two polarities of the bipolar structure observed at 2 cm appear to be aligned along the neutral line of the photospheric magnetic field. The change in polarization during the burst compared to the preburst active-region polarization indicates that during the burst an extra magnetic field emerges from the photosphere, and the flare was probably triggered due to the interaction of this evolving magnetic flux with the quiescent magnetic field of the active region. Triggering of a flare due to the interaction of emerging flux with the field of a quiescent active region has been suggested by Heyvaerts, Priest, and Rust (1977) and suggestive observational evidence for such interaction has been provided by Kundu *et al.* (1982) and Kundu and Shevgaonkar (1985). Due to the bipolar nature of the source and lack of polarization at the maximum of the *I* map, the 2 cm radiation seems to come from the top of the emerging loop.

Following arguments similar to those discussed for the first set of burst peaks, one can show that the 6 cm emission is due to the bulk heated plasma emitting gyrosynchrotron radiation. From Figure 12 it is clear that the emission is optically thick

for a magnetic field greater than 160 G. This means that the absence of polarization at 6 cm provides only a lower limit of ~ 160 G on the magnetic field strength in the emitting region. A better estimate of the magnetic field can come from the observed T_B and the degree of circular polarization at 2 cm. As discussed for the set of I burst peaks, the thermal particles at temperatures ~ 3–7×10^7 K cannot contribute significantly to the burst emission at 2 cm, which should be mainly due to the nonthermal particles trapped near the top of the loop. This indicates that the emitting region consists of bulk heated plasma with the trapped nonthermal particles having power-law energy distribution. A two-component model having a core of nonthermal particles surrounded by a thermal halo has been suggested by Böhme *et al.* (1977) from soft and hard X-ray observations; however, they deduced a relatively high magnetic field of ~ 1500 G in the flaring region.

The brightness temperature of a uniform source having homogeneously mixed thermal and nonthermal particles can be given as

$$T_B = \frac{T_e}{1 + \tau_{NT}/\tau_{TH}} \left\{ 1 - \exp\left[-\tau_{TH}\left(1 + \frac{\tau_{NT}}{\tau_{TH}} \right) \right] \right\} + \frac{T_{eff}}{1 + \tau_{TH}/\tau_{NT}} \left\{ 1 - \exp\left[-\tau_{NT}\left(1 + \frac{\tau_{TH}}{\tau_{NT}} \right) \right] \right\}, \quad (5)$$

where $\tau_{TH} = k_{\nu TH} L$; $\tau_{NT} = k_{\nu NT} L$. L is the linear dimension of the source, and $k_{\nu TH}$, $k_{\nu NT}$, and T_{eff} are given by formulae (1), (2), and (4). Using formula (5), the variation of brightness temperature against the magnetic field is plotted at 6 and 2 cm (Fig. 13) for source parameters $T_e = 10^7$–10^8 K, $B = 100$–600 G, $\theta = 70°$ (appropriate for the source located near the top of the loop at longitude $\sim 30°$), and $\delta = 3$, 3.5, and 4. From Figure 13 it is evident that even in a two-component source model the 6 cm radiation is dominated by optically thick gyrosynchrotron radiation from thermal particles in a magnetic field of greater than ~ 160 G. The 2 cm radiation is optically thin for $B \lesssim 400$ G and becomes thermally optically thick for $B > 400$ G and $\delta \lesssim 3.5$. To get the observed brightness temperature of $\sim 10^6$ K at 2 cm, the value of δ should be between 3.5 and 4, and the magnetic field should be ~ 350 G (cf. Fig. 13). For this magnetic field, since the 2 cm brightness is essentially due to optically thin gyrosynchrotron radiation produced by nonthermal particles, the degree of circular polarization is given by equation (3). Near the top of the loop located at S14W24, taking $\theta \approx 45°$, the degree of polarization should be $\sim 50\%$, which is quite consistent with the observed degree of polarization at 2 cm.

As the eastern source at 2 cm shows enhancement in brightness along with the main burst source, probably there are multiple loops which flare simultaneously. The absence of the 6 cm source corresponding to this eastern component at 2 cm can be explained by assuming that the flaring loop lies lower in the solar atmosphere, and therefore the 6 cm emission is absorbed by the higher optically thick layer of the active region.

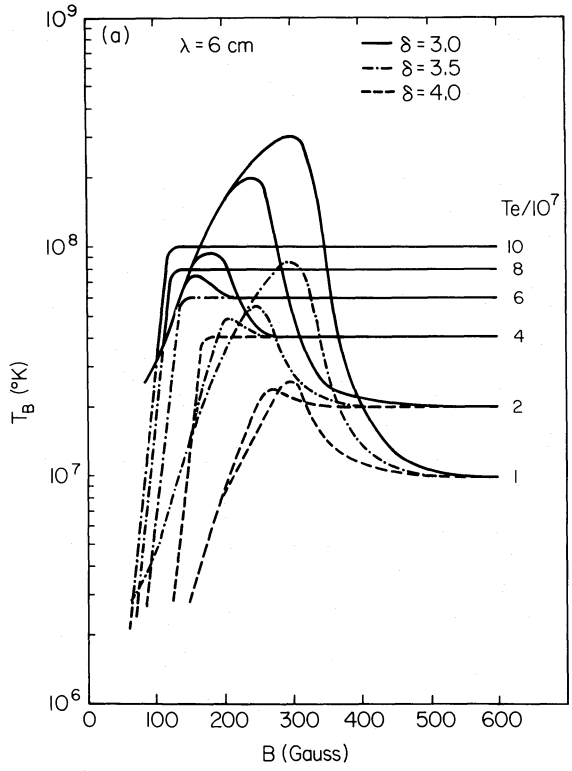

FIG. 13*a*

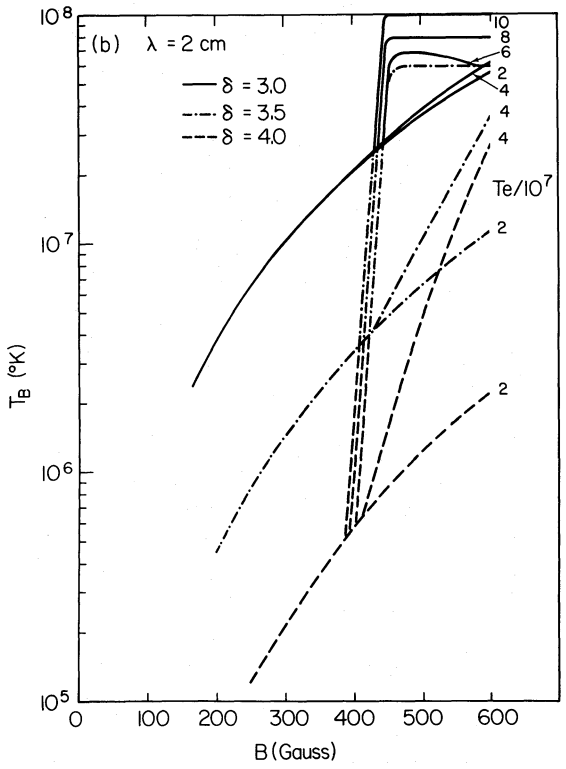

FIG. 13*b*

FIG. 13.—Brightness temperature at (*a*) 6 cm and (*b*) 2 cm from a plasma volume with both thermal and nonthermal particles vs. magnetic field. T_e is the thermal temperature of the plasma and δ is the power-law index of the nonthermal particle energy distribution. The angle between the magnetic field and the line of sight is 70°.

iii) *Time Delays between 2 and 6 cm Burst Peaks*

From Figure 5 it is clear that the two groups of burst peaks have delays of opposite sense between 2 and 6 cm. For the first group (*A*, *B*, *C*) for which the sources at the two wavelengths are not cospatial, the lower frequency emission peaks later. However, for the second group the lower frequency emission peaks earlier than the high frequency emission. It should also be noted that the rise time of all burst components at 2 cm is ~ 30 s and the apparent delay of the 6 cm emission peak must be due to its initial slow rise time. Since the 6 cm burst radiation is believed to be due to gyrosynchrotron radiation from thermal electrons, it should be interesting to investigate whether the delay is related to some characteristic heating time of the plasma.

Brown *et al.* (1983) have tried to explain large delays between the peaks of 5 and 15 GHz emission by a multiple kernel model. In this model the source is assumed to be composed of small kernels with different physical parameters. The small kernels flare sequentially to produce minibursts with much shorter duration. The rise time of an individual miniburst is $\sim L/V_A$ (where L is the kernel size and V_A is the Alfvén velocity), whereas the rise time of the ensemble of the minibursts could be much longer. With a low-temporal-resolution instrument, only the ensemble of the minibursts is observed. Since the different kernels have different physical conditions, they have different spectral characteristics, with the result that the spectral index changes with time. This change in the spectral index during the burst appears in the form of a pseudodelay. Depending upon the physical conditions of the kernels, there may be hardening or softening of the spectrum with time; consequently either type of delay, i.e., high frequency emission peaking later than the lower frequency emission or vice versa, can occur.

Although this model is capable of explaining large delays in either sense, it requires that the physical conditions must change appreciably from one kernel to another. For flares which occupy a large physical area, the presence of kernels with substantially different physical conditions seems possible; however, for compact flares this situation may not be realistic. Further, the multiple-kernel model could apply if the burst emission at the two wavelengths starts simultaneously but their rise times are different. For burst peak *A* (in Fig. 5) and the burst of Figure 9, it is striking that for about 10–20 s after the onset of the 2 cm burst and hard X-ray burst (in Fig. 9), the 6 cm emission rises slowly and then it rises almost as impulsively as the 2 cm emission (see also Shevgaonkar and Kundu 1984). For the burst peaks in the second set (*D*, *E*, *F*), this initial slow-rise phase is absent, and the 6 cm emission starts almost as impulsively as the 2 cm emission.

As discussed earlier, our observations of the two flares are consistent with the general understanding of the impulsive phase of a flare which is characterized by the production of energetic particles and rapid heating of a thermal plasma. Some current solar-flare models propose a high DC electric field to accelerate the particles. The high currents associated with the electric fields in turn produce Joule heating of the thermal plasma (Holman 1984). Since the low-frequency emission (6 cm) is dominated by the emission due to thermal plasma and the high-frequency emission (2 cm) is due to nonthermal particles having a power-law energy distribution, it is worthwhile to see if it is possible to attribute the observed delay to the time difference between the heating of the plasma and the acceleration of the particles (Shevgaonkar and Kundu 1985). Using the relations given by Holman (1985), the Joule heating time (t_J) and the nonthermal particle production time (t_N) are given as

$$t_J = 4 \times 10^{-14} \frac{N_T T_e^{1/2}}{ABv_e} \left(\frac{v_c}{v_e}\right)^2, \quad (6)$$

$$t_N = 1.1 \times 10^{-13} \frac{N_r T_e^{1/2}}{ABv_e} \left(\frac{v_c}{v_e}\right)^{-11/4} \times \exp\left[1.4\left(\frac{v_c}{v_e}\right) + 0.25\left(\frac{v_c}{v_e}\right)^2\right], \quad (7)$$

where v_c = critical velocity = $6(n_e/E)^{1/2}$ (cm s^{-1}), N_T = total number of electrons in the thermal volume $\equiv N_e V$, N_r = total number of accelerated electrons, T_e = thermal temperature of the plasma (K), A = area of the current sheet (cm^2), B = magnetic field (G), v_e = electron thermal velocity = $(kT_e/m_e)^{1/2}$ (cm s^{-1}), v_e = collision frequency in the current sheet $\approx 300 n_e T_e^{-3/2}$ (s^{-1}), n_e = electron density in the current sheet (cm^{-3}), E = DC electric field in the current sheet (statvolt cm^{-1}), and V = volume of the thermal source (cm^3).

Since the 6 cm radiation is due to a thermal plasma and the 2 cm radiation is due to nonthermal particles, t_J and t_N represent the rise times of the 6 and 2 cm emissions. From formulae (6) and (7),

$$\frac{t_J}{t_N} = 0.4 \frac{N_T}{N_r} \left(\frac{v_c}{v_e}\right)^{19/4} \exp\left[-1.4\left(\frac{v_c}{v_e}\right) - 0.25\left(\frac{v_c}{v_e}\right)^2\right]. \quad (8)$$

It is clear from equation (8) that the ratio t_J/t_N could be less than or greater than 1 (i.e., the heating time could be less than or greater than the acceleration time) depending upon the thermal-to-nonthermal particle number ratio (N_T/N_r) and (v_c/v_e). A typical microwave flare requires that 10^{32}–10^{33} electrons be accelerated to energies ~ 100 keV, and from the 6 cm source size ($\sim 10^{27}$ cm^3) and an ambient electron density 10^9–10^{10} cm^{-3}, the total number of thermal particles is $\sim 10^{36}$–10^{37}. This gives an approximate value of N_T/N_r of $\sim 10^4$. Since the 6 cm emission originates from the top of the loop, it is reasonable to assume that the thickness of the thermal source is of the same order as the projected dimension of the source. However, it should be noted that the conclusions derived here do not critically depend on the choice of the source volumes but are rather strongly governed by v_c/v_e. With a value of $(N_T/N_r) \approx 10^4$, for $t_J = t_N$, the value of (v_c/v_e) is ~ 5–6. If $(v_c/v_e) \lesssim 5$ the acceleration time is smaller than the Joule heating time (t_J); on the other hand, it is greater than t_J if $(v_c/v_e) \gtrsim 6$. Therefore, depending on the source parameters (i.e., N_T/N_r, E, n_e, T_e), delays in either sense are possible.

To make a more quantitative analysis of the delays, we consider the two groups of burst peaks separately.

Group I (*A*, *B*, *C*).—From 6 cm observations of the burst peaks *A*, *B*, *C*, and the burst in Figure 9, the volume of the thermal plasma is $\sim 3 \times 10^{26}$ cm^3. If the density in the 6 cm source is $\sim 10^{10}$ cm^{-3}, the total number of thermal particles $N_T \approx 10^{36}$. The relatively unknown parameter is the area of the current sheet, A. Since the bulk heated plasma should be surrounding the current sheet, the area of the current sheet is less than or of the order of the dimension of the bulk heated plasma (6 cm source). Taking the area of the current sheet (A) equal to the area of the 6 cm source, i.e., 5×10^{17} cm^2, and

magnetic field of ~ 160 G (see discussion), the mean rise time is:

$$t_J \approx 15 \times 10^5 v_e^{-1} \left(\frac{v_c}{v_e}\right)^2 . \quad (9)$$

Since t_J is a function of T_e, the mean rise time is at the mean temperature. If the number of nonthermal particles is $\sim 10^{32}$,

$$t_N \approx 350 v_e^{-1} \left(\frac{v_c}{v_e}\right)^{-11/4} \exp\left[1.4\left(\frac{v_c}{v_e}\right) + 0.25\left(\frac{v_c}{v_e}\right)^2\right] . \quad (10)$$

Even if we take $v_c/v_e \approx 2$ (i.e., particles with velocity $\gtrsim 2v_e$ form a nonthermal tail), an electron density of $\sim 2 \times 10^{13}$ cm^{-3} is needed in the current sheet to get the correct order of magnitude for t_J although t_N could be of the right magnitude for lower densities. The other alternatives are (*a*) the presence of a plasma turbulence in the current sheet, creating an anomalous resistivity which is many orders of magnitude higher than the classical value; (*b*) multiple current sheets $\sim 10^4$, as suggested by Holman (1984) to generate nonthermal hard X-rays. However, the multiple current sheet model alone is unable to explain the presence of an initial slow-rise phase compared to the impulsive phase which starts a few seconds later at 6 cm. On the other hand, if the anomalous resistivity is present at the onset of the burst, t_J and $t_N \ll 1$ s; then with a low-temporal-resolution instrument the emissions at both wavelengths will be observed to rise simultaneously, with no delay. This will not explain the initial slow-rise phase observed at 6 cm, however. Therefore, at the very beginning of the burst, the resistivity should be classical. The generation of anomalous resistivity depends on instabilities which are excited if the drift velocity (v_d) of electrons in the current sheet exceeds the threshold velocity $v_{\rm thr} = fC_s$; C_s = ion sound speed (kT_e/m_i) and f is a function of the ratio of electron to ion temperature (T_e/T_i). For $T_e \approx T_i, f \approx 35$; for $T_e \approx 8T_i, f = 8$; and for $T_e \gg 10T_i, f = 1$.

Since $v_{\rm thr} \propto T_e^{1/2}$ and $v_d \propto T_e^{3/2}$ (see Holman 1984), the ratio $v_d/v_{\rm thr} \propto T_e$, i.e., as the temperature increases the ratio $v_d/v_{\rm thr}$ increases, and after a threshold temperature at which $v_d \approx v_{\rm thr}$, the instabilities are induced, the resistivity increases greatly, and the emission at both frequencies increases impulsively. Therefore, during the slow rise phase, to get the correct order of magnitude for the 2 cm rise time, we need $n_e \approx 10^{10}$–10^{11} cm^{-3} in the current sheet. From the relation $v_c/v_e \lesssim 5$ and $v_d/v_{\rm thr} > 1$, we have $10^{-11} \lesssim ET_e/n_e \lesssim 2 \times 10^{-10}$; i e., for $n_e \approx 10^{11}$ cm^{-3} and $T_e \approx 5 \times 10^6$ K (assuming that at this temperature the anomalous resistivity is generated), we can estimate the electric field in the current sheet as $2 \times 10^{-7} \lesssim E \lesssim 4 \times 10^{-6}$ statvolt cm^{-1}.

Group II (*D*, *E*, *F*).—For the second set of burst peaks (*D*, *E*, *F*), the emission at both wavelengths rises impulsively and the rise time at 2 cm is greater than that at 6 cm, i.e., $t_J < t_N$. From equation (8), for $t_J < t_N$, v_c/v_e should be $\gtrsim 6$ if $N_T/N_r \approx 10^4$. For peaks *D*, *E*, and *F* the 2 and 6 cm observations give the volume of the thermal plasma $\sim 10^{27}$ cm^3 and the volume of the nonthermal source $\sim 2 \times 10^{26}$ cm^3. For a density of 10^{10} cm^{-3} for the thermal electrons and a density of $\sim 10^6$ cm^{-3} for the nonthermal electrons, $N_T \approx 10^{37}$ and $N_r \approx 10^{33}$. The estimated magnetic field for these bursts is ~ 350 G. Since (v_c/v_e) is large, for any reasonable value of electron density in the current sheet, t_J and t_N are much larger than the observed rise times if the resistivity is classical and if we assume a single current sheet. Therefore it appears that at the onset of the burst either the anomalous resistivity should be present or the flaring region should consist of many current sheets. If $T_e = T_i$ (i.e., to induce instability $v_d \gtrsim 35C_s$) in the flaring region, the condition for getting anomalous resistivity is

$$\frac{ET_e}{n_e} \gtrsim 2 \times 10^{-10} . \quad (11)$$

Further, if $t_J < t_N$, the condition $v_c/v_e \gtrsim 6$ gives

$$\frac{ET_e}{n_e} \lesssim 0.4 \times 10^{-10} . \quad (12)$$

From equations (11) and (12) it is obvious that the anomalous resistivity cannot be obtained unless $v_{\rm thr}$ is reduced. A reduction in $v_{\rm thr}$ in turn means that $T_e \gg T_i$. Even with this condition, v_c/v_e cannot be higher than ~ 7. If electrons are much hotter than ions ($T_e \gg T_i$), the ion acoustic instability dominates and the collision frequency is (Holman 1984):

$$v_{\rm eff} \approx 300 n_e^{1/2} \ {\rm s}^{-1} . \quad (13)$$

To get a rise time of ~ 30 s at 2 cm, if $n_e \approx 10^{10}$–10^{11} cm^{-3} in the current sheet, (v_c/v_e) should lie between 6 and 7. From equation (12) the estimate of the electric field in the current sheet is $\lesssim 1.3 \times 10^{-7}$ statvolt cm^{-1} if $N_e \approx 10^{10}$ cm^{-3}, and $\lesssim 1.3 \times 10^{-6}$ statvolt cm^{-3} if $N_e \approx 10^{11}$ cm^{-3}.

In the alternative possibility, if we assume the classical resistivity but a large number of current sheets, $\sim 10^4$, there is no lower bound on the strength of the electric field as given by equation (11), and therefore one need not conclude that in the flaring region the electrons are much hotter than the ions.

IV. CONCLUSIONS

a) Active Region

1. The emission at 6 cm is due to gyroresonance absorption and is strongly associated with the sunspots.
2. The edge of the 6 cm source exhibits a higher polarization because away from the center of the source both extraordinary and ordinary modes become optically thin.
3. The peak of the 6 cm radiation is located close to the magnetic neutral line; this indicates that if the emission is associated with magnetic loops it originates from near the tops of the loops.
4. The radiation at 2 cm is in general due to thermal bremsstrahlung. Mostly the extraordinary mode is optically thick, whereas the ordinary mode could be optically thick or thin depending on the strength of the magnetic field in the 2 cm source.
5. The electron density at a height from where the radiation at 2 cm originates is $\gtrsim 10^{10}$ cm^{-3}.

b) Microwave Bursts

1. The 6 cm burst source is located close to the magnetic neutral line of the quiescent active region, whereas the 2 cm source occurs either close to the magnetic neutral line or near the magnetic poles.
2. The 6 cm radiation could be accounted for by the gyrosynchrotron emission due to thermal electrons heated to 3–7×10^7 K.
3. The radiation at 2 cm is associated with nonthermal electrons having a power-law energy distribution. Depending on the density and magnetic field, the 2 cm radiation could be due either to gyrosynchrotron radiation of the nonthermal particles or to low harmonic gyroresonance radiation in the

thermal plasma produced by the thermalization of the nonthermal particles in the dense plasma.

4. From the degree of circular polarization at 2 cm, the magnetic field in the flaring region is estimated to be 160–350 G.

5. The best-fit value of the power-law index δ of the energy distribution of the nonthermal particles is ~ 4.

6. Some of the burst components show emergence of new magnetic structures around the peak.

7. The observations presented here support the two-component model with thermal and nonthermal particles. During the impulsive phase the electrons are accelerated along with the bulk heating of the plasma, but the heating time of the plasma and the nonthermal particle production time could be different.

8. The time delays between the peaks of emission at two wavelengths could be due to the time difference between the heating of plasma and the production of nonthermal particles.

9. Depending on the physical conditions and the strength of the electric field in the current sheet, delays of either sense can be obtained. The magnetic field does not play a dominant role in deciding the value and the sense of the delays.

10. The classical Coulomb resistivity is not always adequate to explain the observations, although a flaring source with multiple current sheets without turbulence can approximately account for the rise time of the burst. During the impulsive phase, along with the large number of current sheets, turbulence could be present to produce anomalous resistivity which is many orders of magnitude higher than the classical value.

11. Delays between the peaks of emission at different wavelength can give an estimate of the electric field if the electron density in the current sheet is known. For an electron density of 10^{11} cm^{-3} the electric field is $0.2 < E < 4$ μstatvolt cm^{-1}.

We thank Dr. G. Holman and Dr. M. Melozzi for useful discussions and critical reading of the manuscript. The National Radio Astronomy Observatory is operated by the Associated Universities, Inc., under contract with the National Science Foundation. This research was supported by NSF grant ATM 81-03089 and NASA grant NGR 21-002-199.

REFERENCES

Alissandrakis, C. E., and Kundu, M. R. 1978, *Ap. J.*, **222**, 342.
Böhme, A., Fürstenberg, F., Hildebrandt, J., Saal, O., Krüger, A., Hoyng, P., and Stevens, G. A. 1977, *Solar Phys.*, **53**, 139.
Brown, J. C., Mackinnon, A. L., Zodi, A. M., and Kaufmann, P. 1983, *Astr. Ap.*, **123**, 10.
Brown, J. C., Melrose, D. B., and Spicer, D. S. 1979, *Ap. J.*, **228**, 592.
Dulk, G. A., and Marsh, K. A. 1982, *Ap. J.*, **259**, 350.
Dulk, G. A., Melrose, D. B., and White, S. M. 1979, *Ap. J.*, **234**, 1137.
Heyvaerts, J., Priest, E. R., and Rust, D. M. 1977, *Ap. J.*, **216**, 123.
Holman, G. D. 1985, *Ap. J.*, **293**, in press.
Kundu, M. R., and Alissandrakis, C. E. 1984, *Solar Phys.*, in press.
Kundu, M. R., Alissandrakis, C. E., Bregman, J. D., and Hin, A. C. 1977, *Ap. J.*, **213**, 178.
Kundu, M. R., Schmahl, E. J., and Velusamy, T. 1982, *Ap. J.*, **253**, 963.
Kundu, M. R., Schmahl, E. J., Velusamy, T., and Vlahos, L. 1982, *Astr. Ap.*, **108**, 188.
Kundu, M. R., and Shevgaonkar, R. K., 1985, *Ap. J.*, **291**, 860.
Kundu, M. R., and Vlahos, L. 1979, *Ap. J.*, **232**, 595.
Lang, K. R., and Willson, R. F. 1983, *Proc. 24th COSPAR, Adv. Space Res. Solar Maximum Year*, ed. Z. Svestka, D. M. Rust, and M. Dryer (New York: Pergamon Press) **2**, 91.
Lang, K. R., Willson, R. F., and Felli, M. 1981, *Ap. J.*, **247**, 338.
Lang, K. R., Willson, R. F., and Gaizauskas, V. 1983, *Ap. J.*, **267**, 455.
Marsh, K. A., and Hurford, G. 1980, *Ap. J. (Letters)*, **240**, L111.
McConnell, D., and Kundu, M. R. 1983, *Ap. J.*, **269**, 698.
Shevgaonkar, R. K., and Kundu, M. R. 1984, *Ap. J.*, **283**, 413.
Shevgaonkar, R. K., and Kundu, M. R. 1985, *Proc. 25th COSPAR, Adv. Space Res., Solar Maximum Data Analysis*, ed. P. Simon (New York: Pergamon Press), in press.
Velusamy, T., and Kundu, M. R., 1981, *Ap. J. (Letters)*, **243**, L103.
———. 1982, *Ap. J.*, **258**, 388.
Willson, R. F., 1983, *Solar Phys.*, **83**, 285.

M. R. KUNDU and R. K. SHEVGAONKAR: Astronomy Program, University of Maryland, College Park, MD 20742